Thin gap approximations for microfluidic device design

Lingyun Ding¹ and Terry Wang¹ and Marcus Roper^{1,2}†

 $^1{\rm Department}$ of Mathematics, University of California, Los Angeles, CA , USA $^2{\rm Department}$ of Computational Medicine, University of California, Los Angeles, CA , USA

(Received xx; revised xx; accepted xx)

Over 125 years ago, Henry Selby Hele-Shaw realized that the depth-averaged flow in thin gap geometries can be closely approximated by two-dimensional (2D) potential flow, in a surprising marriage between the theories of viscous-dominated and inviscid flows. Hele-Shaw flows allow visualization of potential flows over 2D airfoils and also undergird important discoveries in the dynamics of interfacial instabilities and convection, yet they have found little use in modeling flows in microfluidic devices, although these devices often have thin gap geometries. Here, we derive a Hele-Shaw approximation for the flow in the kinds of thin gap geometries created within microfluidic devices. Although these equations have been reported before, prior work used a less direct derivation. Here, we obtain them via a modified Method of Weighted Residuals (MWR), interpreting the Hele-Shaw approximation as the leading term of an orthogonal polynomial expansion that can be systematically extended to higher-order corrections. We provide substantial numerical evidence showing that approximate equations can successfully model real microfluidic and inertial-microfluidic device geometries. By reducing three-dimensional (3D) flows to 2D models, our validated model will allow for accelerated device modeling and design.

Key words: Hele-Shaw approximation; thin-gap flows; microfluidic modeling; inertial effects; 2D approximation; weighted residual methods

1. Introduction

The Hele-Shaw cell, characterized by a narrow gap between two closely spaced parallel plates, is a particularly tractable form of confined flow. Remarkably, flows averaged across the thin gap can be modeled by a 2D potential flow, with the pressure field filling in for the scalar potential. As a result of this tractability, Hele-Shaw geometries can be used to visualize potential flows, such as flow over an airfoil (Fig. 1(a,b)), while serving in their own right as useful models for fundamental interfacial instabilities (Fig. 1c, Saffman & Taylor (1958); Homsy (1987)).

Although Hele-Shaw cells are often thought of as devices for engineering reduced complexity (2D) flows, thin gap domains are also commonly realized in microfluidic devices Stone et al. (2004); Di Carlo (2009), due to the nature of the fabrication methods used to create them. Because the Hele-Shaw approximation can not model no-slip boundary conditions on in-plane boundaries, it has found little use for dissecting the function of existing devices or designing new ones. Yet, it remains unanswered whether a different 2D model from Hele-Shaw exists, allowing the key dynamics present within

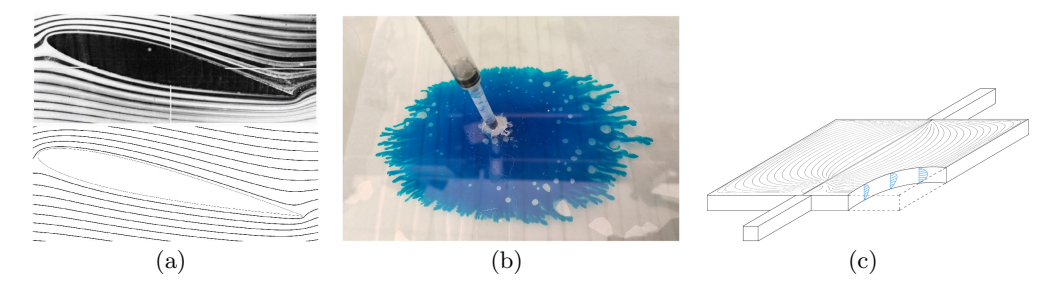


FIGURE 1. The Hele–Shaw approximation models thin-gap flows via 2D potential theory. (a) Streamlines around a model airfoil: top—experiment Werle (1973); bottom—2D potential flow computed in COMSOL 5.4. (b) Thin-gap geometry as a testbed for Saffman–Taylor instability, where a low-viscosity fluid (blue-dyed water) displaces a more viscous one (glycerol). (c) Example microfluidic device with thin gap: a centrifuge-on-a-chip Hur et al. (2011), where a narrow inlet channel feeds a larger rectangular chamber; the assumed parabolic gapwise velocity profile is shown.

a microfluidic or inertial microfluidic device to be predicted or understood, at far less computational cost than a fully 3D flow model.

The classical derivation of Hele-Shaw's approximation assumes that, within the thingap geometry, the flow is planar but varies with z, the gap coordinate. Specifically assuming gap boundaries at $z=\pm\frac{h}{2}$, our putative velocity field is parabolic in z: $\mathbf{u}(x,y,z)\approx (u_1(x,y),v_1(x,y),0)\,6\,(\frac{1}{4}-\frac{z^2}{h^2})$, with $u_1,\,v_1$ the depth averaged velocities. Approximating: $\mu\nabla^2\mathbf{u}\approx\mu\partial^2\mathbf{u}/\partial z^2=-\frac{12\mu}{h^2}(u_1(x,y),v_1(x,y),0)$, and balancing with the pressure gradient, we arrive at a form of Darcy's equation: $(u_1,v_1)=-\frac{h^2}{12\mu}\nabla p$, which models the pressure-driven flow of fluid through a porous medium, when velocities are averaged over multiple pores Whitaker (1986). Assuming that the flow is incompressible, $\nabla\cdot\mathbf{u}=0$, we obtain: $-\nabla^2p=0$, so that the thin gap flow, \mathbf{u} , is a scalar potential flow, and $\frac{h^2p}{12\mu}$ the harmonic potential. Thus, despite the fact that flow between the plates is viscously dominated, the mean flows are captured by the same potential theory that models high-speed inviscid flows, such as those of ideal fluids over airfoils (Fig. 1(a,b)).

The Hele–Shaw approximation captures fluid flows with low complexity, making thingap geometries a useful testbed for studying instabilities such as Saffman–Taylor (Fig. 1c) and Rayleigh–Taylor. Thin gaps are also common in microfluidic devices, which manipulate and analyze nanoliter volumes of fluid, but two key deficits limit the approximation's applicability. It accounts only for the no-through-flow effect of rigid boundaries, treating no-slip as confined to an unmodeled O(h) region near the boundary. It also neglects fluid inertia, which thickens boundary layers to O(Reh) and creates new regimes that enable sorting and segregation of particles and droplets Di Carlo (2009).

Previous work has aimed to incorporate these additional effects into Hele-Shaw-type models. One approach involves adding boundary layer corrections Balsa (1998), though these calculations are often complex and highly geometry-dependent. Another direction is to modify the governing equations themselves. The Darcy-Brinkman equations add inplane viscous stresses to Darcy's law, Brinkman (1949), and can be used for porous media Tsay & Weinbaum (1991); Howells (1974), as well as to thin-gap geometries with empirically determined relative coefficients on the in-plane and in-depth stresses Pepper et al. (2010). There are, by contrast, multiple pathways for incorporating inertial effects. When modeling porous media flow, a nonlinear pressure-flow relation (Darcy-Forchheimer) is commonly imposed Chen et al. (2001); Guta & Sundar (2010). Conversely, when Darcy's law is arrived at by integrating the flow equations over some thin dimension, inertia-

containing terms may likewise be integrated, though there are disagreements between papers on the precise coefficients thereby obtained Desvillettes *et al.* (2008); Inamdar *et al.* (2020).

Here, we arrive at a Hele Shaw-like approximation via a systematic expansion of the flow-field in the gap coordinate. Our approximation naturally includes inertial and inplane viscous stresses. Comparisons with full 3D simulations shows that our approximation accurately models flows in geometries used in real microfluidic devices, including both conventional (Re = 0) and inertial (Re = 1 - 100) microfluidic flows.

2. A new perspective of the Hele-Shaw approximation

We consider the Navier-Stokes equations for an incompressible, homogeneous fluid confined within a uniform-thickness gap. The equations are non-dimensionalized using the gap height h, so that the vertical coordinate z lies in the interval -1/2 < z < 1/2. We expand the velocity field as a series, $\mathbf{u} = \sum_{i=1}^{\infty} \mathbf{u}_i(x,y)Q_i(z)$. We impose a noslip boundary condition on \mathbf{u}_i on any in-plane boundaries. Because the Hele-Shaw approximation yields a parabolic profile for the in-plane velocity components in the narrow gap limit, we select $Q_1(z) = z^2 - 1/4$ as the leading vertical basis function. Moreover, because all velocity components must vanish at the boundaries $z = \pm 1/2$, a natural choice for the basis that captures the vertical variation is the Gegenbauer (ultraspherical) polynomials with parameter $\alpha = -1/2$ Belinsky (2000), shifted to the domain -1/2 < z < 1/2: $Q_n(z) = \frac{1}{2} \int_{-1}^{2z} P_n(\zeta) d\zeta$, where P_n is the *n*-th Legendre polynomial. We obtain a sequence of basis functions: $Q_1 = (z^2 - 1/4), Q_2 = 2z(z^2 - 1/4),$ $Q_3 = (5z^2 - 1/4)(z^2 - 1/4)$. Projection of our equations onto this basis benefits from the fact that $\langle Q_m, Q_n \rangle = 0$ for $m \neq 0$, where $\langle f, g \rangle \equiv \int_{-1/2}^{1/2} f(z)g(z)(1/4-z^2)^{-1} dz$. However, when the series expansion of u is substituted into the Navier-Stokes equations, there is no way to isolate the terms in Q_1 from higher order polynomial contributions. As a first step toward resolving this closure problem, we consider applying the series expansion to a unidirectional shear flow (rectilinear flow).

Poiseuille flow: We first consider pressure-driven flow in a channel, aligned with the x-axis, with uniform rectangular cross-section $(y, z) \in [-L/2, L/2] \times [-1/2, 1/2]$. Supposing an imposed pressure gradient of G, and scaling p_x by G, and velocities by Gh^2/μ , the steady-state Navier-Stokes equations is (u(y, z), 0, 0), where u satisfies a 2D Poisson equation $(\partial_y^2 + \partial_z^2)u = -1$. In the rectangular channel, this equation admits a Fourier series solution, first derived by Boussinesq (1868). By substituting the leading order forms of the components of \mathbf{u} into the Poisson equation, we obtain:

$$6\left(\frac{1}{4} - z^2\right)u_1'' - 12u_1 + 1 \approx 0, (2.1)$$

where the first two terms come from Δ , and the third term is the dimensionless pressure gradient. Including additional bases such as Q_3, Q_4, \ldots in our expansion would allow us to eliminate the z-dependent terms in Eq. (2.1), but at the expense of introducing a coupled system of equations for the unknown functions u_i . Before considering the more complex coupled system, we first seek an optimal closure involving only u_1 . We assume the optimal closure is of the form: $au_1'' - 12u_1 + 1 = 0$ for some constant, a, to be determined. Substituting into Eq. (2.1) leads to $r(z;a)u_1''(y) \approx 0$, where $r(z;a) = 6\left(\frac{1}{4} - z^2\right) - a$. Since $u_1''(y) = 0$ produces only trivial solutions, we choose a to minimize the left-hand side,

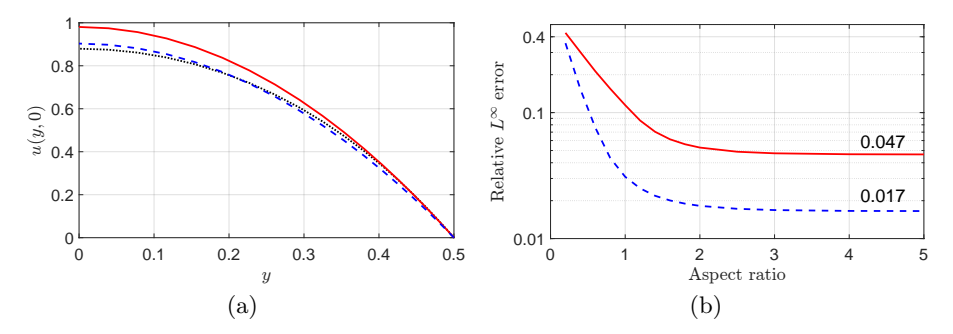


FIGURE 2. Validating a 2D approximation for the pressure-driven flow in a rectangular channel. (a) Flow profile at z=0: exact solution (black curve), approximation from Eq. (2.3) (red curve), and approximation from Eq. (2.5) (blue dashed curve), for L=1. (b) Relative error, measured by the L^{∞} norm $\frac{\|u-u_{\rm app}\|_{\infty}}{\|u\|_{\infty}}$, as a function of aspect ratio L. Red curve: Eq. (2.3), blue dashed curve: Eq. (2.5).

integrating the squared residual against a weight function w(z):

$$E(a; w) \equiv \int_{-\frac{1}{2}}^{\frac{1}{2}} \left(6\left(\frac{1}{4} - z^2\right) - a \right)^2 w(z) dz.$$
 (2.2)

Choosing w(z) = 1, yields $E(a; 1) = a^2 - 2a + \frac{6}{5}$, which is minimized by a = 1, thereby recovering the Darcy-Brinkman approximation, and its solution

$$u_1(y) = -\frac{\left(1 - \cosh(\sqrt{12}y) \operatorname{sech}(L\sqrt{3})\right)}{2} \left(\frac{1}{4} - z^2\right).$$
 (2.3)

The key step to producing a better approximation is to observe that the space of functions spanned by Gegenbauer polynomials remains the natural space in which to optimize our approximation of Eq. (2.1). Since terms in Eq. (2.1) do not vanish at $z = \pm 1/2$, we multiply the equation by a weight $w(z) = (1/4 - z^2)$. Then $r(z; a)w(z) = \sum_m \beta_m Q_m$, for some set of coefficients β_m , and applying Parseval's theorem to this series expansion gives:

$$E(a; w) \equiv \int_{-1/2}^{1/2} r(z; a)^2 (1/4 - z^2) dz = \langle w(z)r, w(z)r \rangle = \sum_m \beta_m^2 \langle Q_m, Q_m \rangle^2.$$
 (2.4)

Therefore, our optimal closure consists of minimizing Eq. (2.2) with $w(z) = (1/4 - z^2)$. Under this weight, we obtain $E(a; w) = a^2/6 - 2a/5 + 9/35$, which is minimized when a = 6/5. This optimal closure leads to a different optimal profile:

$$u_1(y) = -\frac{\left(1 - \cosh(\sqrt{10}y)\operatorname{sech}\left(L\sqrt{\frac{5}{2}}\right)\right)}{2}\left(\frac{1}{4} - z^2\right). \tag{2.5}$$

Both approximations derived above are compared against the exact solution. The choice a=6/5 consistently yields a more accurate approximation across the entire y-domain (Fig. 2a) and for all tested values of L (Fig. 2b). For example, when L=1, the relative errors for a=1 and a=6/5 are 0.115 and 0.031, respectively. The accuracy of the a=6/5 approximation is particularly noteworthy, given that L=1 does not satisfy the classical scale-separation assumption $L\gg 1$. As L increases beyond 1, the relative error decreases rapidly for both approximations, indicating convergence toward

the asymptotic limit. To probe the optimality of our closure relation more closely, at each aspect ratio, we numerically compute the error-minimizing value of a (determined by minimizing the relative L^{∞} error between approximate and exact velocity profiles): for aspect ratio 1, the value of a is 1.196; for aspect ratio 3, it is 1.188; and for aspect ratio 5, it is 1.184. Hence, the value a = 6/5 = 1.2 we obtained by minimizing the residual, closely approximates the optimal error-minimizing values.

Our closure method follows the general framework of MWR Finlayson (2013). In the standard application of MWR to obtain a reduced-order model for a differential equation $\mathcal{L}(u) = f$, one begins by selecting a set of basis functions $\phi_i(z)_{i=1}^N$ and approximating the solution as $u(x,z) \approx \sum_{i=1}^N u_i(y)\phi_i(z)$. The residual is then defined as $r(y,z) = \mathcal{L}(u(y,z)) - f(y,z)$. A set of weight functions $w_j(z)_{j=1}^N$ is chosen, and the residual is projected onto these weights via $\int_{\Omega} w_j(z)r(y,z)\mathrm{d}z = 0, j = 1, \ldots, N$, yielding a system of N equations for the unknown coefficients $u_i(y)$. Our modification lies in the third step: rather than integrating the equation against multiple orthogonal weights, we assume a closure equation with unknown parameters, substitute it into the residual, and determine the parameters by minimizing the weighted L^2 norm of the resulting expression. This approach offers greater flexibility in the form of the closure equation.

Ideally, if minimizing the residual directly yielded an optimal approximation to the true solution—without requiring the original equation to be solved—this would be a highly desirable outcome. However, this is not generally the case. In our example (Fig. 2), the near-optimal approximation results from a carefully chosen combination of basis functions and residual metric that reflect the underlying physical behavior of the system. We use Gegenbauer polynomials as basis functions, motivated by the parabolic profile of the classical Hele-Shaw approximation. The weighted L^2 norm used for residual minimization is chosen to align with the orthogonality properties of these polynomials.

Stokes flow in coaxial flow devices: Under the assumption of Stokes flow, the nonlinear term $\mathbf{u} \cdot \nabla \mathbf{u}$ is again negligible. The optimal 2D approximation replaces the operator Δ by $a\Delta_H - 12$, where $\Delta_H \equiv \partial_x^2 + \partial_y^2$, even when the flow is three dimensional. The same choice of a may be justified (residuals such Eq. (2.2)) are obtained for each component of the fully 3D Stokes flow). The residual analysis of the continuity equation yields $\partial_x u_1 + \partial_u v_1 = 0$. We test the approximation on a thin-gap but non-rectilinear flow that is commonly realized in microfluidic devices. In coaxial flow, three fluid streams, flowing sufficiently slowly that Re = 0, are combined and pass through a narrow aperture (Fig. 3a, Anna et al. (2003)), emerging as a inner fluid thread sandwiched between the outer fluids. In real coaxial flow devices, the surface tension of the inner fluid thread breaks it up into droplets. We consider a version of the coaxial flow experiment without viscosity contrasts or surface tension, focusing only on the ability of the optimal 2D model to render the geometry of the interface between the inner and outer fluids. We used COMSOL Multiphysics 5.4 to solve both the 3D Stokes equations and the 2D approximate models, and to compare their streamlines with those from the optimal 2D approximation.

Simulations were performed using the geometry from Anna $et\ al.\ (2003)$, while varying the mass flux ratio Q between the inner and outer flows. At a representative value of Q, (Fig. 3b), the optimal 2D approximation with a=6/5 closely approximates the interface in both the narrowing and diverging sections of the channel, whereas the classical Hele-Shaw approximation (a=0) overpredicts the downstream width of the middle layer, and provides only qualitative agreement in shape. The agreement between the 2D approximation and the full 3D computation in the far downstream region is expected for two reasons. First, the flow becomes rectilinear, resembling Poiseuille flow—a regime

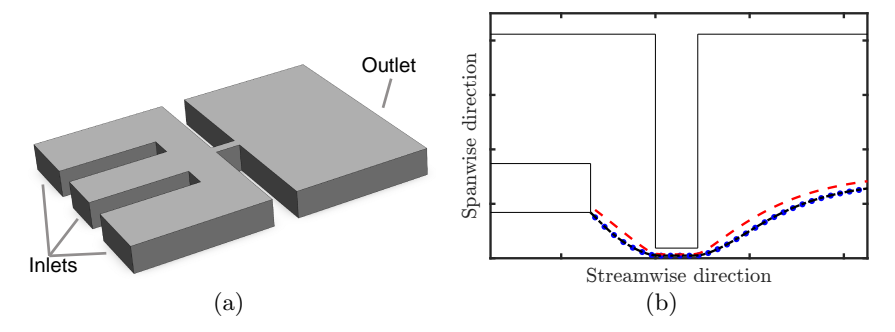


FIGURE 3. Coaxial flow. (a) Simulation geometry based on Anna *et al.* (2003): left— inlets, right- outlet. Outer inlets have mass flux Q, the inner inlet has flux 1. Inlet and outlet lengths are extended by 20 to ensure fully developed flow. (b) Dividing streamlines for Q=1.7: classical Hele–Shaw (red), derived a=6/5 approximation (blue dotted), and 3D simulation (black dashed).

in which our optimal 2D approximation is already known to be accurate (Fig. 2b). Second, mass conservation between the inlets and the outlet constrains the position of the interfaces within the downstream Poiseuille flow. Indeed, it is unsurprising that the classical Hele-Shaw approximation will over-predict the width of the inner-jet (Fig. 3b), because it treats the downstream flow as uniform or plug-like in y, omitting the slowdown near the sidewalls of the channel that prevents narrowing of the outer flows. However, the optimal 2D approximation renders the interface accurately even where the flow passes through the narrow orifice separating the inlets and outlet. Although the orifice is relatively narrow (aspect ratio, width:depth < 0.4), and conventional wisdom holds that Hele-Shaw-type models are accurate only when the channel is much wider (aspect ratio $\gtrsim 1$), the optimal 2D approximation still performs well. Remarkably, the flow remains approximately two-dimensional even within the orifice: the ratio of out-ofplane to in-plane velocity components peaks at just 0.22. This modest degree of threedimensionality, forced by the thin gap geometry, suggests that the validity of our optimal 2D model extends well beyond the classical limits typically associated with the Hele-Shaw approximation.

3. Thin gap flows at moderate Reynolds numbers

After validating the accuracy of the approximation for Stokes flow (i.e. for thin gap microfluidic devices), we can generalize it to the case of thin gap flows at moderate Reynolds numbers. These conditions are often realized in inertial microfluidic devices, which are commonly built using the same soft-lithography techniques, and similar dimensions to regular microfluidic devices, but are perfused with high pressure pumps, to create \sim m/s flows Di Carlo (2009).

For the finite Reynolds number flow, we incorporate an extra term into our closure equation:

$$\operatorname{Re}(a\partial_{t}\mathbf{u}_{H} + b\mathbf{u}_{H} \cdot \nabla_{H}\mathbf{u}_{H}) = c\Delta_{H}\mathbf{u}_{H} - d\mathbf{u}_{H} - \nabla_{H}p, \ \nabla_{H} \cdot \mathbf{u}_{H} = 0, \ \mathbf{u}_{H}|_{\partial\Omega} = 0.$$
 (3.1)

Following the same weighted residual analysis, using the weight functions $w(z) = \frac{1}{4} - z^2$

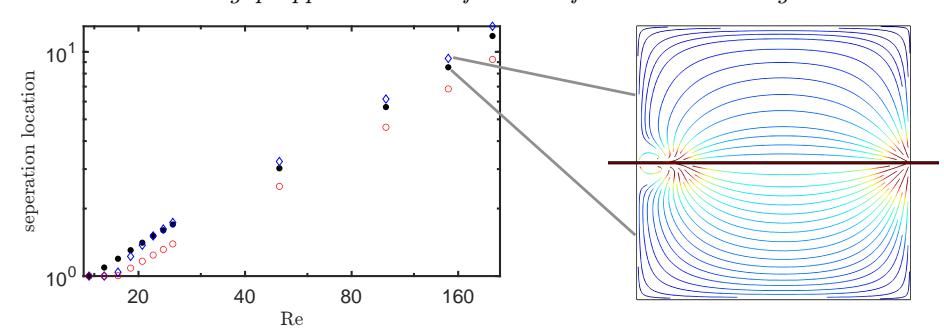


FIGURE 4. 2D approximation for finite Re flows in a centrifuge-on-a-chip geometry. Comparison of the separation bubble width in 3D simulation (black), 2D approximation (blue, Eq. (3.2a)), and unweighted residual approximation (red, Eq. (3.2b)). Right panels: Streamline patterns colored by velocity magnitude (red = larger, blue = smaller), comparing the 2D approximation (top) with the full 3D simulation (bottom).

and w(z) = 1 yields the following sets of coefficients, respectively:

$$(a,b,c,d) = \left(\frac{6}{5}, \frac{54}{35}, \frac{6}{5}, 12\right),\tag{3.2a}$$

$$(a, b, c, d) = \left(1, \frac{6}{5}, 1, 12\right).$$
 (3.2b)

Previous work has reported these and similar closure models, arrived at by different approximations and techniques. For example, Plouraboué & Hinch (2002); Yuan & Azaiez (2014) used $a=1,\ b=1,\ c=1,$ and d=12, while for the case of Stokes flow, Zeng et al. (2003) proposed $a=b=0,\ c=\frac{12}{\pi^2}\approx 1.21,$ and d=12. The closure equation with w(z)=1 coefficients was derived in Gondret & Rabaud (1997) by assuming a parabolic flow profile, and averaging the Navier-Stokes equations across the gap.

By positing an expansion of the velocity fields as a (non-spectral) sequence of polynomials, and matching powers of z, Ruyer-Quil (2001) derived a version of the closure equation with values $a=\frac{6}{5},\ b=\frac{54}{35},\ c=0$, and d=12. Although it omits in-plane viscous stresses, this model has found wide use in studies of fluid instability in Hele-Shaw geometries Chevalier et al. (2006). Martin et al. (2002) add in-plane viscous stresses with an effective viscosity to this model resulting in identical coefficients to Eq. (3.2a). More recently, Li et al. (2021) arrived at the same 2D approximation as (3.2a), via a lubrication approximation approach, viz. systematic expansion of all pressure and velocity fields in powers of h/L. By calculating terms up to $O(h^2/L^2)$, and neglecting terms proportional to the square of the Reynolds number, they arrive at Eq. (3.2a). We do not therefore make any claim to be the first to arrive at this 2D approximation, but note that optimal closure via MWR provides a direct and physically transparent route to deriving the equation.

To test our 2D approximation and to compare weighted and unweighted residuals, we compare both 2D approximations with 3D simulations of flow in a centrifuge-on-a-chip (Fig. 1c), which consists of a rectangular chamber connected to two narrow, elongated channels serving as the inlet and outlet Hur et al. (2011). In our simulations, performed in COMSOL Multiphysics 6.3, the chamber occupies $(x,y,z) \in [-50,50] \times [-50,50] \times [-0.5,0.5]$, while the inlet and outlet have unit square cross-sections. The inlet region of the flow resembles the channel expansion on which Li et al. (2021) have already validated the 2D approximation (3.2a), but the centrifuge-on-a-chip is a paradigmatic example of the design of inertial microfluidic devices to fractionate particles, such as cells in a blood sample, by size, so centrifuge-on-a-chip flows merit separate attention.

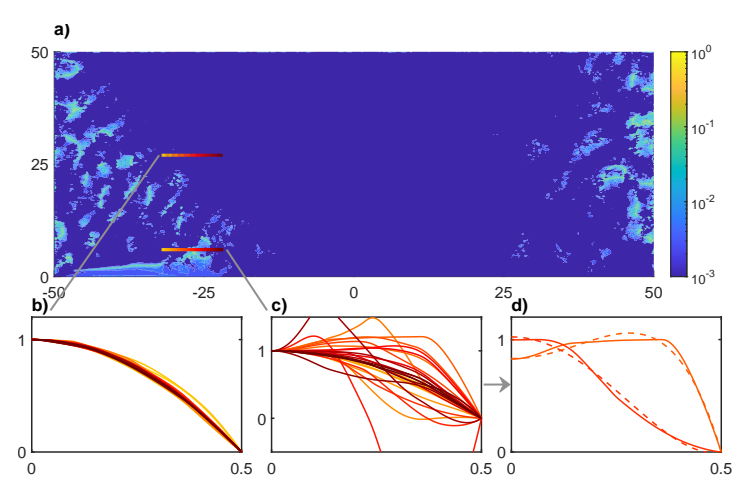


FIGURE 5. Fidelity of the numerically computed 3D flow field to the Hele-Shaw (parabolic flow profile) for a centrifuge-on-a-chip flow. (a) r (defined in Eq. (4.1)) at Re = 200 across the centrifuge chamber. (b,c) u- profiles against z sampled on two different transects (locations shown in (a)). To compare shapes, all profiles are normalized so that u=1 at z=0 (b) shows a small r-region, where the Hele-Shaw approximation is valid, and (c) a region on the boundary of the inlet jet, where it is not. Line colors give x-ordinates. (d) Adding Q_3 to our basis allows non-Hele-Shaw features to be rendered. Two specific non-parabolic velocity profiles from the y=6 transect are shown (solid lines) along with their projections onto Q_1 and Q_3 (dotted line). Simulations were performed in COMSOL Multiphysics 6.2, with P2+P2 elements and the extra fine mesh further refined to ensure a maximum cell length of 0.1.

As the Reynolds number $\text{Re} = Uh/\nu$ of the inlet flow is increased, a separation eddy forms at the centrifuge entrance, and this eddy plays a role in trapping of large particles Paiè et al. (2017). We measure the eddy size by interpolating the v=0 contour to the wall x=-50. The 2D approximation (3.2a) (left panel, blue diamonds) models the growth of the 3D eddy with Re (black circles), better than the unweighted residual model (red circles) (3.2b). Though both approximations slightly overpredict the value of Re at which separation first occurs (17.5 compared to 16 for the fully 3D simulation), the unweighted residual approximation underestimates the separation eddy size by a factor of 16-21% over the entire Re-range (Fig. 4), while the error from our 2D approximation (3.2a) never exceeds 12%. Comparing flow fields (Fig.4, right panel), we see that the 2D approximation from (3.2a) also quantitatively matches the streamlines and velocities obtained in 3D simulations.

4. Breakdown of the 2D model

Although the 2D approximation (3.2a) shows good accord with 3D simulations, there is mild disagreement in flow features such as eddy size. The framework used to derive the approximation naturally lends itself to determining where and how the approximation breaks down. In forming our approximation we have adopted the Hele-Shaw approximation of assuming a parabolic velocity profile across the gap, and no fluid velocity in the depth direction. Based on Fig. 4, we focus particularly on dissecting the features of moderate Reynolds number flows that cause these approximations to break down. We first studied whether the assumption of zero vertical velocity breaks down. Across the entire centrifuge-on-a-chip and for every value of Re that we simulated, the flow is nearly two-dimensional: the largest value of $|w|_{\infty}/|\mathbf{u}|_{\infty}$ we observe is only 0.0555, obtained in the chamber outlet.

We then investigate whether the assumption of a parabolic velocity breaks down. We define a non-parabolicity quantifier for the x-component of the velocity field:

$$r := \frac{|\langle u, \overline{Q_3} \rangle|}{\sqrt{\langle u, \overline{Q_1} \rangle^2 + \langle u, \overline{Q_3} \rangle^2}}, \quad \overline{Q_k} \equiv Q_k / \sqrt{\langle Q_k, Q_k \rangle}. \tag{4.1}$$

r measures the relative contribution of the third and first modes to the Gegenbauer polynomials expansion of u(x,y,z). A larger value of r indicates a greater deviation from the parabolic profile. r values remain small ($\lesssim 10^{-2}$) throughout most of the centrifuge-on-a-chip even at Re = 200. Moderate values (up to $10^{-1} - 1$) occur, in small patches distributed on both the proximal and distal walls of the chamber and more coherently in a jet of fluid entering the centrifuge via the inlet channel (Fig. 5). Inlet jets are common features of moderate to high-Reynolds number flows, and are associated with the inertia of the fluid entering the centrifuge chamber, which doesn't decelerate to 0 until the jet has penetrate a distance ≈ 25 into the centrifuge. The presence of the jet violates the Hele-Shaw assumption in two regards: 1. There is a thin boundary layer in the xy-plane between the jet and the nearly still fluid in the chamber, and 2. the flow profile is non-parabolic with shear that is closely localized near the $z = \pm 1/2$ walls (Fig. 5b).

Our coaxial jet results (Fig.3 b) show that narrow x- or y-dimensions alone do not break the thin-gap approximation; the main limitation is its inability to represent non-parabolic profiles. A natural remedy is to add higher-order terms to the asymptotic expansion. Including just one extra term (e.g., Q_3) markedly improves accuracy, and a two-term expansion reproduces all velocity profiles observed across the jet boundary layer (Fig.5d). While the parabolic form cannot capture non-convex or boundary-layer shapes, the two-term projection resolves both.

5. Discussion

We introduced a modified MWR to derive optimal closure equations, interpreting the Hele–Shaw approximation as the leading term of an orthogonal polynomial expansion for the velocity. This framework reproduces a previously derived approximation Martin *et al.* (2002); Li *et al.* (2021) through a simpler, more direct dominant-term analysis, while naturally extending to higher-order corrections.

What benefit can be gained from higher-order approximations? First, in many microfluidic thin-gap flows, the vertical velocity remains small, making truly 3D flows rare in thin-gap geometries. Conversely, truly 2D flows occur only in special cases, such as Stokes flow in a channel with constant radius of curvature Lauga *et al.* (2004). Some applications, however, deliberately induce strong three-dimensionality, e.g. micromixing Stroock *et al.* (2002). In such cases, using a higher-order leading form for w from our orthogonal polynomials, e.g., $w = w_1(x,y)(Q_4(z) - Q_2(z))$, can improve accuracy, but yields coupled PDEs without a straightforward closure. Second, higher-order terms provide a built-in mechanism for estimating and controlling approximation error. If the estimated error exceeds a chosen tolerance, additional terms can be systematically added to improve accuracy.

While our analysis primarily focused on the fluid velocity equation, the approach is flexible and broadly applicable. It can be readily extended to other physical quantities, such as solute concentration, electric fields, and magnetic fields, arising in applications like reactive solute transport Salmon & Ajdari (2007), electrokinetic flows Lin *et al.* (2008); Ding (2023), and magnetohydrodynamic microfluidics Qian & Bau (2009). The method also allows for generalization of boundary conditions—for example, incorporating no-

stress boundaries to model bubble motion Booth *et al.* (2025) or flows in microchannels with soft walls Inamdar *et al.* (2020).

The authors acknowledge financial support from NSF award DMS-2009317 (to MR). **Declaration of interests.** The authors report no conflict of interest.

REFERENCES

- Anna, Shelley L, Bontoux, Nathalie & Stone, Howard A 2003 Formation of dispersions using "flow focusing" in microchannels. *Appl. Phys. Lett.* 82, 364–366.
- Balsa, Thomas F 1998 Secondary flow in a hele-shaw cell. *Journal of Fluid Mechanics* **372**, 25–44.
- Belinsky, Rachel 2000 Integrals of legendre polynomials and solution of some partial differential equations. *Journal of Applied Analysis* 6 (2), 259–282.
- BOOTH, DJ, GRIFFITHS, IM & HOWELL, PD 2025 The motion of a bubble in a non-uniform hele-shaw flow. *Proceedings of the Royal Society A* **481** (2311), 20240613.
- BOUSSINESQ, JOSEPH 1868 Mémoire sur l'influence des frottements dans les mouvements réguliers des fluids. Journal de Mathématiques Pures et Appliquées 13 (2), 377–424.
- BRINKMAN, HENDRIK C 1949 A calculation of the viscous force exerted by a flowing fluid on a dense swarm of particles. Flow, Turbulence and Combustion 1 (1), 27–34.
- Chen, Zhangxin, Lyons, Stephen L & Qin, Guan 2001 Derivation of the forchheimer law via homogenization. Transport in porous media 44, 325–335.
- Chevalier, Christophe, Amar, Martine Ben, Bonn, Daniel & Lindner, Anke 2006 Inertial effects on saffman—taylor viscous fingering. *Journal of fluid mechanics* **552**, 83–97.
- CORNISH, R Jo 1928 Flow in a pipe of rectangular cross-section. Proceedings of the Royal Society of London. Series A, Containing Papers of a Mathematical and Physical Character 120 (786), 691–700.
- DESVILLETTES, LAURENT, GOLSE, FRANÇOIS & RICCI, VALERIA 2008 The mean-field limit for solid particles in a navier-stokes flow. *Journal of Statistical Physics* **131**, 941–967.
- DI CARLO, DINO 2009 Inertial microfluidics. Lab on a Chip 9 (21), 3038–3046.
- DING, LINGYUN 2023 Shear dispersion of multispecies electrolyte solutions in the channel domain. *Journal of Fluid Mechanics* **970**, A27.
- FINLAYSON, BRUCE A 2013 The method of weighted residuals and variational principles. SIAM. GONDRET, PHILIPPE & RABAUD, MARC 1997 Shear instability of two-fluid parallel flow in a
- GONDRET, PHILIPPE & RABAUD, MARC 1997 Shear instability of two-fluid parallel flow in a hele–shaw cell. *Physics of Fluids* **9** (11), 3267–3274.
- Guta, Lemi & Sundar, S 2010 Navier-stokes-brinkman system for interaction of viscous waves with a submerged porous structure. *Tamkang journal of mathematics* **41** (3), 217–243.
- Homsy, George M 1987 Viscous fingering in porous media. *Annual review of fluid mechanics* 19 (1), 271–311.
- HOWELLS, ID 1974 Drag due to the motion of a newtonian fluid through a sparse random array of small fixed rigid objects. *Journal of Fluid Mechanics* **64** (3), 449–476.
- Hur, Soojung Claire, Mach, Albert J & Di Carlo, Dino 2011 High-throughput size-based rare cell enrichment using microscale vortices. $Biomicrofluidics\ 5\ (2)$.
- INAMDAR, TANMAY C, WANG, XIAOJIA & CHRISTOV, IVAN C 2020 Unsteady fluid-structure interactions in a soft-walled microchannel: A one-dimensional lubrication model for finite reynolds number. *Physical Review Fluids* **5** (6), 064101.
- Lauga, Eric, Stroock, Abraham D & Stone, Howard A 2004 Three-dimensional flows in slowly varying planar geometries. Physics of fluids ${\bf 16}$ (8), 3051–3062.
- LI, DI, SONG, LE, ZHANG, CHENG, YU, LIANDONG & XUAN, XIANGCHUN 2021 A depth-averaged model for newtonian fluid flows in shallow microchannels. *Physics of Fluids* 33 (1).
- LIN, HAO, STOREY, BRIAN D & SANTIAGO, JUAN G 2008 A depth-averaged electrokinetic flow model for shallow microchannels. *Journal of Fluid Mechanics* **608**, 43–70.
- MARTIN, J, RAKOTOMALALA, N & SALIN, D 2002 Gravitational instability of miscible fluids in a hele-shaw cell. *Physics of Fluids* **14** (2), 902–905.
- Paiè, P, Che, J & Di Carlo, D 2017 Effect of reservoir geometry on vortex trapping of cancer cells. *Microfluidics and Nanofluidics* 21, 1–11.

- Pepper, Rachel E, Roper, Marcus, Ryu, Sangjin, Matsudaira, Paul & Stone, Howard A 2010 Nearby boundaries create eddies near microscopic filter feeders. *Journal of the Royal Society Interface* **7** (46), 851–862.
- PLOURABOUÉ, FRANCK & HINCH, E JOHN 2002 Kelvin-helmholtz instability in a hele-shaw cell. *Physics of Fluids* **14** (3), 922–929.
- QIAN, SHIZHI & BAU, HAIM H 2009 Magneto-hydrodynamics based microfluidics. *Mechanics research communications* **36** (1), 10–21.
- RUYER-QUIL, CHRISTIAN 2001 Inertial corrections to the darcy law in a hele–shaw cell. Comptes Rendus de l'Académie des Sciences-Series IIB-Mechanics 329 (5), 337–342.
- SAFFMAN, PHILIP GEOFFREY & TAYLOR, GEOFFREY INGRAM 1958 The penetration of a fluid into a porous medium or hele-shaw cell containing a more viscous liquid. *Proceedings of the Royal Society of London. Series A. Mathematical and Physical Sciences* **245** (1242), 312–329.
- Salmon, Jean-Baptiste & Ajdari, Armand 2007 Transverse transport of solutes between co-flowing pressure-driven streams for microfluidic studies of diffusion/reaction processes. *Journal of applied physics* **101** (7).
- STONE, HOWARD A, STROOCK, ABRAHAM D & AJDARI, ARMAND 2004 Engineering flows in small devices: microfluidics toward a lab-on-a-chip. Annu. Rev. Fluid Mech. 36, 381–411.
- Stroock, Abraham D, Dertinger, Stephan KW, Ajdari, Armand, Mezic, Igor, Stone, Howard A & Whitesides, George M 2002 Chaotic mixer for microchannels. *Science* **295** (5555), 647–651.
- TSAY, RUEY-YUG & WEINBAUM, SHELDON 1991 Viscous flow in a channel with periodic cross-bridging fibres: exact solutions and brinkman approximation. *Journal of Fluid Mechanics* **226**, 125–148.
- WERLE, H 1973 Hydrodynamic flow visualization. Annual Review of Fluid Mechanics 5 (Volume 5, 1973), 361–386.
- WHITAKER, STEPHEN 1986 Flow in porous media i: A theoretical derivation of darcy's law. Transport in porous media 1, 3–25.
- Yuan, Qingwang & Azaiez, Jalel 2014 Inertial effects of miscible viscous fingering in a hele-shaw cell. Fluid Dynamics Research 47 (1), 015506.
- ZENG, JIE, YORTSOS, YANNIS C & SALIN, DOMINIQUE 2003 On the brinkman correction in unidirectional hele-shaw flows. *Physics of Fluids* **15** (12), 3829–3836.